한국소음진동공학회 1995년도 추계학술대회논문집 pp. 62-67

부구조물이 있는 유한길이의 쉘 구조물에서의 충격하중에의한 음향방사

최 성훈*

(Acoustic Radiation from a Finite-length Shell with Substructures Subjected to an Impulsive Load)

(Sung-Hoon Choi)

1.INTRODUCTION

Shell structures submerged in a fluid are often subjected to time harmonic or impulsive vibration forces. Several authors have already investigated the harmonic excitation of submerged shells. It is well known that an analytic solution exists if the outer shell geometry conforms to a separable coordinate system. For other geometries, a numerical approach is needed. The most widely employed numerical methods are based on boundary or finite element techniques, in which the surface response is expressed in terms of local shape functions. Some of the methods are summarized in a recent survey by Chien *et al.* [1]. An alternative method using global shape functions, developed by Wu [2] and Ginsberg *et al.* [3], uses a variational method to determine the relationship between the surface pressure and surface velocity for axisymmetric bodies. Several papers since then have progressively extended the generality of the formulation [4-6]. The variational principle formulation has been proven to be an effective basis for studying the effects of substructures in capped cylinders on acoustic radiation [7,8].

Time domain analysis provides insight into the radiation phenomena that can not be seen in the frequency domain. Keer *et al.* [9] studied the transient response of an elastic shell using Laplace and Fourier transforms. Stepanishen and Ebebezer [10] investigated the transient response of finite cylinders in an infinite rigid baffle subjected to axisymmetric excitations. Kaduchak and Marston [11] used a ray method to study the time domain scattering of tone bursts by spherical shells. Wahl and Bolton [12] presented a method by which the fast Fourier transformation algorithm can be used to predict the response of line-excited, fluid-loaded panels. Brévart and Fuller [13] studied the impulsive response of fluid-filled elastic cylindrical shells of infinite length using a double Fourier transformation in the wave number and frequency domains. They demonstrated the contributions of various waves to the structural response and their propagation path by evaluating individual pole contributions to the total responses. Utschig [14] used the same approach to find the impulsive response of an infinitely long submerged cylindrical shell. He also studied the effect of a spring-mass substructure on the near-field pressure response. Mann *et al.* [15] analyzed the vibrational energy of capped cylinders using data from near-field acoustical holography measurements. They examined the exchange of energy between the shell and the acoustic field for finite time duration forces. In many of these studies [11, 12, 14, 15], the fast Fourier transform has proven to be an effective method to approximate the response in the time domain.

The purpose of the present paper is to investigate the response of capped cylindrical shells subjected to impulsive loads. First, the equations of motion for harmonic excitations are derived based on a Lagrange energy formulation. A variational principle is used to determine the impedance relations between the surface pressure and the surface velocity of the shell. Then, the responses evaluated at a discrete set of frequencies are transformed to the time domain using a Fast Fourier Transform technique to obtain impulsive responses. The proposed method is very efficient in such problems where responses at many closely spaced frequencies are required. The response of a capped cylindrical shell is compared with that of an infinite fluid-loaded cylindrical shell. The effects of bulkhead substructures on the near-field response are also investigated. The contributions of the elastic waves, the driving force and the bulkhead/shell interaction to the near-field pressure are exhibited. Physical interpretations of the results in terms of energy exchange between the shell and the surrounding fluid are presented.

* 삼성종합기술원

2. FORMULATION OF EQUATIONS OF MOTION

The main structure considered in this paper is in the shape of an arbitrary body of revolution. Internals to the shell are axisymmetric substructures which are connected to the shell. The shell is subjected to a time-harmonic loading. In this section, the $e^{-i\omega t}$ term, where ω is the circular frequency and t is time, will be omitted for convenience with the understanding that all harmonic response expressions are to be multiplied by this term.

First, the arc-length parameter, s, is defined such that $s = -s_m$ and $s = s_m$ correspond to the ends of the shell. The shape of the axisymmetric shell is described in parametric form by functions $r(s)$ and $z(s)$, which are the coordinates of the generating curve in the radial and axial directions, normalized with respect to the cylindrical shell radius a. The position vector of each point on the shell is described by $\mathbf{x} = \mathbf{x}(s,\theta)$, where θ is the azimuthal angle.

The derivation of the governing equations starts with an expansion of the surface pressure and displacement using global shape functions. For an axisymmetric shell geometry one can use Fourier series expansions to represent the θ dependence of all variables. The s dependence is expanded in a series of basis functions. To develop a non-dimensional representation, we scale the displacement by the radius a and the pressure by ρc^2, where ρ and c are the fluid mass density and sound speed, respectively. Thus the pressure p and displacement $\mathbf{w}$ of the shell are written as

$$p(\mathbf{x},t) = \rho c^2 \sum_{n=0}^{N_c} \sum_{m=1}^{N_p} p_{mn} \psi_{mn}(s) \cos n\theta \tag{1}$$

$$\mathbf{w}(\mathbf{x},t) = a \sum_{n=0}^{N_c} \sum_{m=1}^{N_w} w_{mn} \boldsymbol{\phi}_{mn}(s) \cos(n\theta - \theta_x) \tag{2}$$

where p_{mn} and w_{mn} are modal amplitudes and $\psi_{mn}(s)$ and $\boldsymbol{\phi}_{mn}(s)$ are the pressure and displacement basis functions. The displacement of the k-th substructure is expanded as

$$u_k(r,\theta) = a \sum_{n=0}^{N_c} \sum_{j=1}^{J_k} u_{jn,k} \upsilon_{jn,k}(r) \cos(n\theta - \theta_x) \tag{3}$$

where $u_{jn,k}$ are modal coordinates and the $\upsilon_{jn,k}(r)$ are the in-vacuo modes of the k-th substructure with free boundary conditions. The displacement basis functions have three components which correspond to the displacements tangential and normal to the shell surface. Herein, bold lower case letters are used to denote such three-component vectors.

The number of circumferential modes, N_c, and the number of basis functions, N_p and N_w, are chosen to be sufficiently large such that the contribution of the last term in the series is several orders of magnitude smaller than the entire sum. One of the virtues of the variational principle is that, once a sufficient number of mode is included in the expansions for the surface pressure and displacement fields, convergence is extremely rapid.

In the present paper, the natural modes of the dry shell will be used for displacement basis functions $\phi_{mn}(s)$ and a Fourier series will be used for the pressure basis functions $\psi_{mn}(s)$. Also only driving forces symmetric about $\theta = 0$ will be considered. Hence, the cosine series expansion is used for the pressure and displacement fields which are symmetric with respect to $\theta = 0$ and the sine series expansion is used for the circumferential displacement field which is anti-symmetric. In Eq.(2) the phase angle θ_s is used to express the different dependence on θ of the two circumferential expansions. The value of θ_s is $\pi/2$ for the circumferential displacement and zero otherwise.

To construct Lagrange's equations, the kinetic and potential energy terms for the shell and substructures, and the work done by the applied harmonic loading are first derived. The constraints are specified by equating the displacements and rotations of the shell and substructures at their connections. Since the internal substructures are axisymmetric the connections are circular arcs defined by $\mathbf{x} = \mathbf{x}_k(s_k,\theta)$. The constraint conditions are given by

$$\mathbf{f}_k = \sum_{n=0}^{\tau}\left\{\sum_{m=1}^{N_w} w_{mn}\begin{bmatrix}\phi_{mn}(s_k)\\ \nabla\times\phi_{mn}(s_k)\end{bmatrix} - \sum_{j=1}^{J_k} u_{jn,k}\begin{bmatrix}\upsilon_{jn,k}(a)\\ \nabla\times\upsilon_{jn,k}(a)\end{bmatrix}\right\}\cos(n\theta-\theta_s) = 0 \tag{4}$$

for $k = 1,2,\cdots,K$. Equation (12) holds for every circumferential mode number n, hence one can rewrite it as

$$\mathbf{f}_{n,k} = \mathbf{c}_{n,k}^{\mathrm{T}}\mathbf{w}_n - \mathbf{c}_{n,k}^{s\,\mathrm{T}}\mathbf{w}_n \tag{5}$$

where $\mathbf{w}_n = \left\{w_{1n} \cdots w_{N_w n}\right\}^{\mathrm{T}}$ and $\mathbf{u}_{n,k} = \left\{u_{1n,k} \cdots u_{J_k n,k}\right\}^{\mathrm{T}}$ are vectors of displacement coefficients for the shell and the k-th substructure. The components of the matrix $\mathbf{c}_{n,k}$ and $\mathbf{c}^s_{n,k}$ are given by

$$\mathbf{c}_{n,k} = \begin{bmatrix}\phi_{1n}(s_k) & \nabla\times\phi_{1n}(s_k)\\ \cdots & \cdots\\ \phi_{Nn}(s_k) & \nabla\times\phi_{Nn}(s_k)\end{bmatrix}$$

and (6)

$$\mathbf{c}^s_{n,k} = \begin{bmatrix}\upsilon_{1n,k}(a) & \nabla\times\upsilon_{1n,k}(a)\\ \cdots & \cdots\\ \upsilon_{Jn,k}(a) & \nabla\times\upsilon_{Jn,k}(a)\end{bmatrix}$$

Following standard procedures for the derivation of Lagrange's equations, the Lagrangian L_n can now be constructed as

$$L_n = T_n - V_n - U_n^e - U_n^f + \Lambda_n\cdot\mathbf{f}_n \tag{7}$$

for each circumferential harmonic n, where T_n and V_n are the kinetic and potential energies of the shell/substructure system, Λ_n is a vector of Lagrange multipliers and $\mathbf{f}_n = \left[\mathbf{f}_{n,1}^{\mathrm{T}} \cdots \mathbf{f}_{n,K}^{\mathrm{T}}\right]^{\mathrm{T}}$ is a vector of constraint conditions. It is possible to write the Lagrange's equations for each circumferential harmonic because the circumferential expansions are orthogonal for axisymmetric geometries and the energy expressions decouple for each circumferential mode n. The work done on the shell by external forces consists of two parts: the work U_n^e done by an external harmonic pressure excitation $\mathbf{q}^e(s,\theta)$ and the work U_n^f done by the fluid pressure. The work quantities are given by

$$U_n^e = \rho c^2 a^3\sum_{m=1}^{N_w} q_{mn}^e w_{mn} \tag{8}$$

and

$$U_n^f = \rho c^2 a^3\sum_{m=1}^{N_w} q_{mn}^f w_{mn} \tag{9}$$

Here q_{mn}^e and q_{mn}^f are the generalized forces for the external and fluid loading, given by

$$q_{mn}^e = \int_{-\pi}^{\pi}\int_{-s_m}^{s_m}\left[\mathbf{q}^e(s,\theta)\cdot\phi_{mn}(s)\right]\cos(n\theta-\theta s)r(s)ds d\theta \tag{10}$$

and

$$q_{mn}^f = -\sum_{l=1}^{N_p} R_{ml,n}p_{ln} \tag{11}$$

where $R_{ml,n}$ are displacement-pressure coupling coefficients defined by

$$R_{ml,n} = \pi\varepsilon_n\int_{-s_m}^{s_m}\psi_{ln}(s)\left[\mathbf{n}(s)\cdot\phi_{mn}(s)\right]r(s)ds \tag{12}$$

Here $\varepsilon_n = 1 + \delta_{n0}$ and δ_{ij} denotes the Kronecker delta. Lagrange's equations can now be written as

$$\frac{d}{dt}\left(\frac{\partial L_n}{\partial\dot{q}_j}\right) - \frac{\partial L_n}{\partial q_j} = 0 \tag{13}$$

Here, the generalized coordinates q_j are given by w_{mn}, $u_{mn,k}$ and the components of Λ_n. But he system of equations derived by using Eq. (13) is not complete, since the fluid loading term is still unknown.

Now, the variational principle formulation [2-8] will be used to obtain a relationship between the surface pressure and surface displacement. The relation between the unknown surface pressure and displacement is given for each circumferential harmonic, n, as

$$\mathbf{A}_n\mathbf{p}_n = \mathbf{B}_n\mathbf{w}_n \tag{14}$$

where $\mathbf{p}_n = \left\{p_{1n} \quad p_{2n} \quad \cdots \quad p_{N_p n}\right\}^{\mathrm{T}}$ is a vector of surface pressure coefficients. The elements of matrices $\mathbf{A}_n$ and $\mathbf{B}_n$ are given in the Reference [8].

Applying Eq. (13) yields a complete set of simultaneous equations for the combined shell/substructure system:

$$\begin{bmatrix}\mathbf{A}_n & -\mathbf{B}_n & \mathbf{0} & \mathbf{0}\\ \mathbf{R}_n & \mathbf{D}_n & \mathbf{0} & \mathbf{C}_n\\ \mathbf{0} & \mathbf{0} & \mathbf{D}_n^s & -\mathbf{C}_n^s\\ \mathbf{0} & \mathbf{C}_n^{\mathrm{T}} & -\mathbf{C}_n^{s\,\mathrm{T}} & \mathbf{0}\end{bmatrix}\begin{bmatrix}\mathbf{p}_n\\ \mathbf{w}_n\\ \mathbf{u}_n\\ \Lambda_n\end{bmatrix} = \begin{bmatrix}\mathbf{0}\\ \mathbf{q}_n^e\\ \mathbf{0}\\ \mathbf{0}\end{bmatrix} \tag{18}$$

The submatrices and subvectors in the above equation are related in an obvious manner to the coefficients defined previously. The elements of the matrices $\mathbf{C}_n$ and $\mathbf{C}_n^s$ are given by

$$\mathbf{C}_n = \left[\mathbf{c}_{n,1} \quad \mathbf{c}_{n,2} \quad \cdots \quad \mathbf{c}_{n,K}\right],\quad \mathbf{C}_n^s = \left[\mathbf{c}_{1,q}^s \quad \mathbf{c}_{n,2}^s \quad \cdots \quad \mathbf{c}_{n,K}^s\right] \tag{19}$$

The matrix $\mathbf{D}_n$ is diagonal with elements defined as

$$D_{ij,n} = \frac{a^2}{c^2}M_{in}\left(\omega_{in}^2 - \omega^2\right)\delta_{ij} \tag{20}$$

where M_{mn} and ω_{mn} are modal masses and natural frequencies of the dry shell. The matrix $\mathbf{D}_n^s$ represents the substructure equations written as

$$\mathbf{D}_n^s = \begin{bmatrix}\mathbf{D}_{n,1}^s & & \mathbf{0}\\ & \mathbf{D}_{n,1}^s & \\ \mathbf{0} & \cdots & \\ & & \mathbf{D}_{n,K}^s\end{bmatrix} \tag{21}$$

with its submatrices given by

$$\mathbf{D}_{ijn,k}^s = \frac{a^2}{c^2}M_{in,k}\left(\omega_{in,k}^2 - \omega^2\right)\delta_{ij} \tag{22}$$

in which $M_{in,k}$ and $\omega_{in,k}$ are modal masses and natural frequencies of the *k-th* substructure. The system of equations (18) offers a solution of the problem at hand, simultaneously solving for the vector of surface pressure coefficients, the shell and substructures modal coordinates and the vector of Lagrange multipliers. After Eq. (18) has been solved for each n, the pressure and displacement coefficients are substituted

into Eqs. (1) and (2) to obtain the surface pressure and displacement.

3. FFT IMPLEMENTATION

To find the response (pressure or displacement) of a shell in the time domain, it is necessary to perform inverse Fourier transforms. Let $p(\mathbf{x},ka)$ be the response in the space-frequency domain and $\tilde{p}(\mathbf{x},\tau)$ be its transformation pair in the space-time domain, where $ka = \omega a/c$ is a non-dimensional frequency parameter and $\tau = tc/a$ is a non-dimensional time. The inverse integral can be numerically evaluated by using the inverse fast Fourier transform. Using the method described in the previous section, the response in the frequency domain is first evaluated at increments of Δka over a range $[0{:}ka_{max}]$. The frequency spectra are then extended to the negative frequency range so that they are complex conjugate symmetric about $ka = 0$. The result of the fast Fourier transform is then a real time sequence with time increment $\Delta\tau = \pi / ka_{max}$ representing the response due to a short duration load.

One of the side effects in using the FFT are the side lobes in the input force which make the response more difficult to interpret. To reduce the side lobes, the response spectra of the input is weighted by a filter, defined by $F(ka) = \cos^2[\pi(ka/ka_{max})]$ which is usually called a "hanning window" [16]. With this frequency filter, the maximum side lobes decreases to -32dB below the main lobe, while the main lobe width nearly doubles.

The use of the FFT creates another source of error, which is often referred to as aliasing or "wrap-around" error. This error occurs as a result of the inherent assumption in the FFT algorithm that the data record is periodic. A sufficiently small frequency step Δka is necessary to avoid this aliasing phenomenon on the time period of interest. This is especially true for lightly damped structures. The inverted time sequence can be enhanced by zero-padding. The time sequence of the zero-padded signal contains no new information but provides an interpolation of the original time sequence. In the following analysis the frequency spectra are expanded to $[-\overline{ka}_{max} : \overline{ka}_{max}]$ by zero padding and the new time interval is $\Delta\tau = \pi / \overline{ka}_{max}$. For the example studies in the next section, the original calculation are performed for frequencies from $ka = 0.005$ to 10.0 with a frequency step $\Delta ka = 0.005$. The response spectra are then extended to the negative frequency range and zero-padded to result in a total of 16,384 frequency values in the range [-40.96: 40.96].

4. EXAMPLE STUDY

To demonstrate the method, a finite-length shell with a cylindrical mid-section and hemispherical endcaps is considered (Fig. 1). The shell is modeled as a steel structure submerged in water. The ratio of the mass densities of the shell and water is 7.84:1. The ratio of the overall shell length to the radius is 12:1 and the ratio of the cylinder radius to the wall thickness is 50:1. The internal substructures consist of two bulkheads, modeled as circular plates of thickness $0.25a$ attached rigidly to the shell at $s = 1.5$. The bulkheads generate radial, longitudinal and circumferential forces and bending moments at the connections. Structural damping is introduced by assigning a complex value to the elastic modulus such that $E = E_0(1 - i\eta)$, where E_0 is the nominal real-valued modulus and η is the loss factor. A loss factor of 0.04 is used for both the shell and the substructures. In-vacuo modes of a shell and a circular plate are used for displacement basis functions and a set of sinusoidal functions are used for pressure basis functions. Details on the shape functions are given in previous papers [7,8]. Two different kinds of forces are considered in the example study: a line force described by a function $f(\tau)\delta(s)\cos(n\theta)$ and a point force described by $f(\tau)\delta(s)\delta(\theta)$.

4.1 PRESSURE FIELD

First, the surface pressure response of an empty shell subjected to an axisymmetric ring force ($n = 0$) is presented as a series of snapshots in time (Fig. 2). For comparison, the same snapshots have also been generated for an infinitely long cylindrical shell with periodic ring forces spaced at intervals of $2s_m a$. These benchmark results are computed using a modal-based solution given in Ref. [17]. In Fig. 4 one finds that the surface pressure responses coincide almost

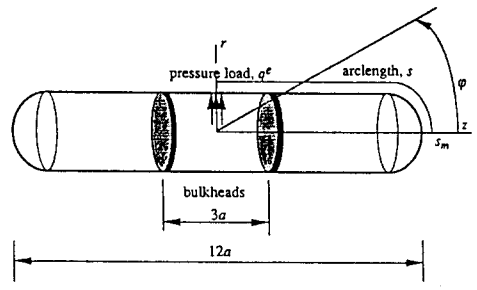

Figure 1. Example problem geometry.

exactly for time $\tau \le 6.75$. For these figures, the shell flexural waves have not yet reached the endcap. Although the faster longitudinal waves have already reached the endcap, these waves have small radial components as compared to the flexural waves and generate relatively small surface pressure. The most significant pressure generated by the longitudinal wave occurs at the endcap because of the effects of curvature [18]. This is observed in Fig. 4 at time $\tau = 2.15$ where a slight pressure disturbance appears at the endcap portion of the shell. The surface pressure response of a finite shell starts to deviate significantly from that of an infinite shell after the flexural waves reaches the endcap portion. At larger times, the waves travel around the shell and the amplitude level decays due to the radiation and structural damping.

The pressure field in the surrounding fluid can be calculated directly from the Kirchhoff-Helmholtz integral. The pressure fields in the fluid are presented as snapshots in time using density plots where the horizontal axis is the axial distance z/a and the vertical axis is the radial distance r/a. In Figs. 3-5(a) are shown the near-field pressure generated from an empty shell subjected to an impulsive ring load. The near-field pressure for a shell with bulkheads are also calculated and the difference in pressure fields generated by shells with and without bulkheads are presented in Figs. 3-5(b). The time $\tau = 0.00$

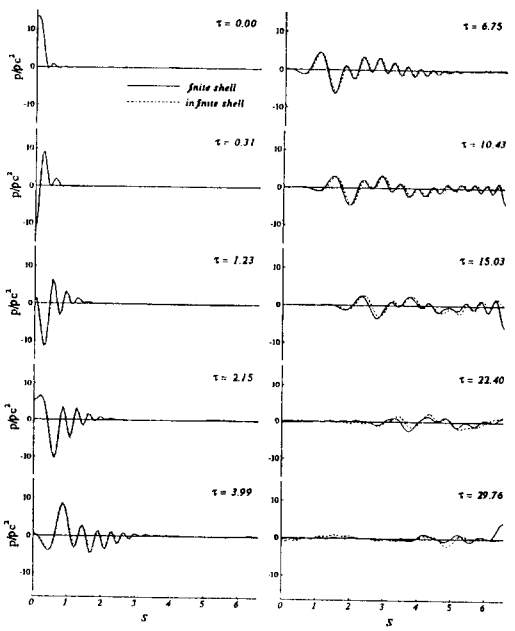

Figure 2. Surface pressure along the arc-length parameter s of an empty finite length shell (solid lines) and an infinite cylindrical shell (dashed lines).

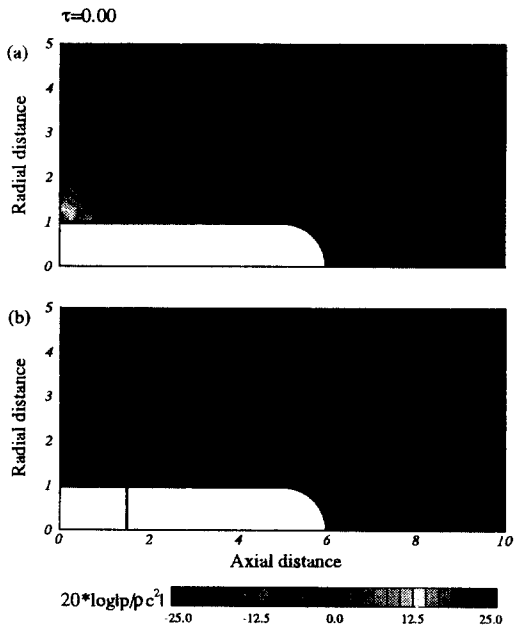

Figure 3. Near-field pressure distribution in the r-z plane at τ = 0.00. (a) empty shell; (b) difference in pressure due to bulkheads.

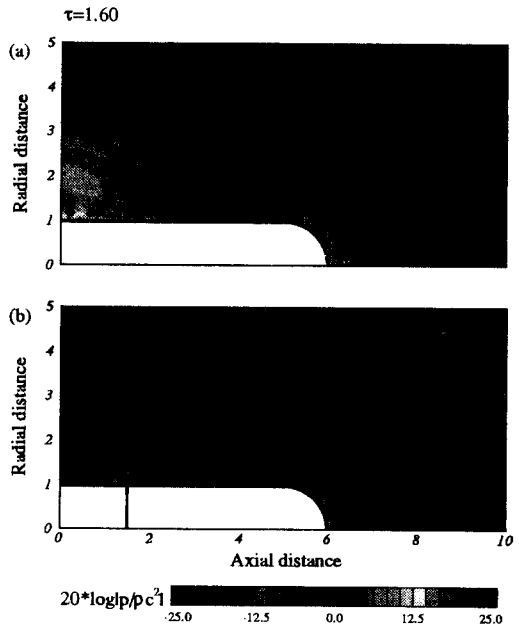

Figure 4. Near-field pressure distribution in the r-z plane at τ = 1.60. (a) empty shell; (b) difference in pressure due to bulkheads.

corresponds to the peak of the impulse. Since the driving force is not a perfect impulse the pressure field at $\tau = 0$ is already spread over a span of the shell and into the fluid. The near-field pressure consists of contributions from the elastic waves on the shell and those from the direct radiation from the drive point. The direct radiation is identified as a circular arc centered at the drive point. The structure borne waves are generated in the fluid by flexural waves propagating in the shell surface, as seen in Fig. 5(a). These structure borne waves are

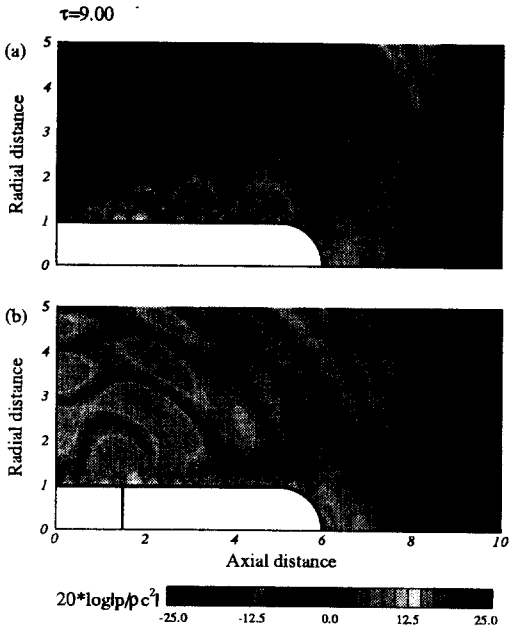

Figure 5. Near-field pressure distribution in the r-z plane at τ = 9.00. (a) empty shell; (b) difference in pressure due to bulkheads.

evanescent, decaying exponentially away from the shell surface. This is because the shell flexural waves are predominantly subsonic [19]. A pressure field is also generated by the longitudinal waves. At time τ = 1.60, the longitudinal waves hit the cylinder/endcap interface, couple to transverse vibrations of the endcap, and produces radiating acoustic waves as shown in Fig. 4(a). The effect of the bulkheads on the pressure fields, as shown in Fig. 5(b), is due to the interaction forces at the connection point. Direct radiation from the connection point as well as from the evanescent structure borne waves, due to the reflected and transmitted shell waves, can be observed.

4.2 ENERGY IN THE SYSTEM

An alternative approach in terms of intensity will be presented in the next section. This analysis will provide interesting results to understand energy exchange between the shell and the surrounding fluid medium.

The instantaneous intensity normal to the shell surface is defined as

$$I_n(\mathbf{x},t) = p(\mathbf{x},t)\mathbf{n}(\mathbf{x}) \cdot \mathbf{w}(\mathbf{x},t) \tag{23}$$

this represents the flux of energy propagating through the point $\mathbf{x}$ in the direction normal to the shell surface. A positive value of the instantaneous intensity means that the shell injects energy into the fluid while a negative value means that the fluid injects energy back into the shell. The total energy that passes through a point is calculated by time-integrating Eq. (23). The instantaneous intensity and time-integrated intensity have been calculated for the finite shell subjected to a point impulse at $s = 0$ and $\theta = 0$. In Fig. 6 are shown the instantaneous and time-integrated intensity at two different points on the shell, one at the drive point and the other at the endcap. At first, the shell and fluid exchange energy, but then the instantaneous intensity approaches zero because the vibration of the shell decays to zero due to damping. The time-integrated intensity curves show that the net energy flows from the shell to the fluid at the drive point and flows from the fluid to the shell at $s = 6$. Figure 6(b) shows that the time-integrated intensity becomes negative which indicates that more energy re-enters to the shell. This phenomenon happens for most points on the shell except near the drive point. It is also observed that the intensity level decays rapidly to a very low level at the endcap.

The total energy radiated into the acoustic medium can be calculated by integrating the time-integrated intensity over the entire shell surface. The total energies radiated from the shell subjected to point impulses, with and without bulkheads, are presented in Fig. 7. The total energy input, which is simply the integration of the force multiplied by the shell velocity at the drive point, is also calculated. One can observe that the radiated energy reaches a maximum soon after the impulse occurs and decays to an asymptotic value. After the vibration energy decays to zero, the total input energy is equal to the sum of the energy radiated into the fluid and the energy dissipated in the shell by damping. Figure 7 shows that 0.91% of the energy input is radiated from the empty shell and 2.23% is radiated from the shell with bulkheads. This result is consistent with the results reported in a previous paper [8] that the waves generated at the bulkhead connections have radiating supersonic components. Figures 8(a) and (b) show for each circumferential harmonic, n, the net energy input

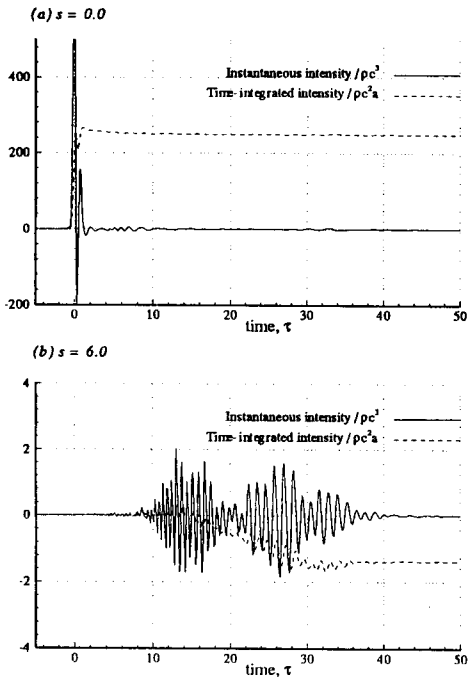

Figure 6. Time history of instantaneous intensity and time-integrated intensity. (a) $s = 0.0$; (b) $s = 6.0$.

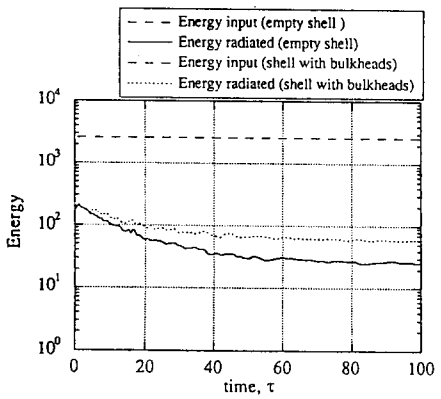

Figure 7. Net energy input and energy radiated for an empty shell and a shell with bulkheads.

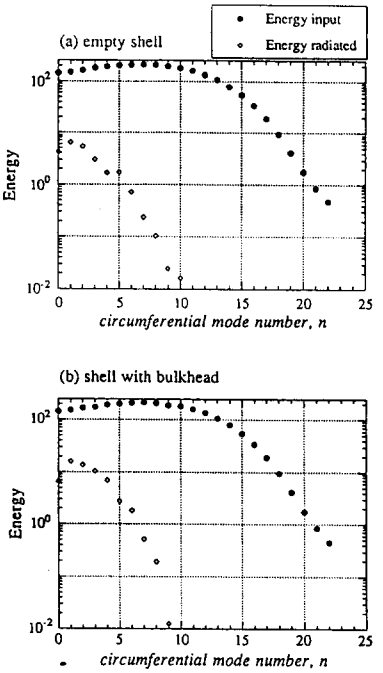

Figure 8. Net energy input and energy radiated for each circumferencial mode number. (a) empty shell; (b) shell with bulkheads.

and energy radiated from the shell with and without bulkheads. These figures show that almost all of the energy is radiated through the lower circumferential harmonics ($0 \le n \le 6$). The beam mode ($n = 1$) is seen to be the most efficient radiating mode. It is also seen that very little energy is injected to the system when $n \ge 20$. This is because the lower cut-off frequencies for these modes are higher than the dominant input frequencies.

5. CONCLUSIONS

A method for determining impulsive responses and acoustic radiation for submerged shells of finite length has been presented. The method is a modal-based method, and uses a surface variational principle to obtain data in the frequency domain. The fast Fourier transform technique is used to convert the data to the time domain.

The surface pressure responses of a cylindrical shell with endcaps were compared with those of an infinite shell. It was shown that the surface pressures coincide exactly before any significant reflections from the endcaps occur. Traces of different types of waves were identified from the dispersion relations of the infinite shell. The contributions of flexural and longitudinal waves and these due to the direct radiation from the driving force to the fluid pressure were demonstrated using near-field plots. The exchange of energy between the shell and fluid was examined for shells with and without bulkheads. It was shown that a significant amount of the energy which enters the fluid returns to the shell and most of the energy is dissipated in the shell. It was also shown that the shell with bulkheads radiate significantly more energy into the far-field than the empty shell.

REFERENCES

[1] C. C. Chien, H. Rajiyah, and S. N. Atluri, "An effective method for solving hyper-singular integral equations in 3-D acoustics," J. Acoust. Soc. Am. **88**, 918-937 (1990).

[2] X.-F. Wu, "Faster calculation of sound radiation from vibrating cylinders using variational principles," J. Vib. Acoust. Stress. Reliab. Des. **111**, 101-107 (1989).

[3] J. H. Ginsberg, P.-T. Chen, and A. D. Pierce, "Analysis using variational principles of the surface pressure and displacement along

an axisymmetrically excited disk in a baffle," J. Acoust. Soc. Am. **88**, 548-559 (1990).

[4] J. H. Ginsberg and J. G. McDaniel, "An acoustic variational principle and component mode synthesis applied to the analysis of acoustic radiation from a concentrically stiffened plates," J. Vib. Acoust. **113**, 401-408 (1991).

[5] J. H. Ginsberg and P. Chu, "Asymmetric vibration of a heavily fluid-loaded circular plate using variational principles," J. Acoust. Soc. Am. **91**, 894-906 (1992).

[6] P.-T. Chen and J. H. Ginsberg, "Variational formulation of acoustic radiation from submerged spheroidal shells," J. Acoust. Soc. Am. **94**, 221-233 (1993).

[7] J. Bjarnason, T. Igusa, S.-H. Choi, and J. D. Achenbach, "The effect of sub-structures on the acoustic radiation from axisymmetric shells of finite length," J. Acoust. Soc. Am. **96**, 246-255 (1994).

[8] S.-H. Choi, T. Igusa, and J. D. Achenbach, "Nonaxisymmetric vibration and acoustic radiation of a submerged cylindrical shell of finite length containing internal substructures," J. Acoust. Soc. Am. **98**, 353-362 (1995).

[9] L. M. Keer, J. F. Fleming, and G. Herrmann, "Transient response of an elastic shell in plane strain," J. Acoust. Soc. Am. **41**, 358-368 (1967).

[10] P. R. Stepanishen and D. D. Ebebezer, "Transient vibratory response of fluid-loaded shells with axisymmetric excitations," J. Acoust. Soc. Am. **82**, 1811-1817 (1987).

[11] G. Kaduchak and P. L. Marston, "Backscattering of chirped bursts by a thin spherical shell near the coincidence frequenccy," J. Acoust. Soc. Am. **93**, 2700-2706 (1993).

[12] T. J. Wahl and J. S. Bolton, "The use of Fourier transforms to calculate the spatial and temporal response of line-driven, layer-wise homogeneous acoustically loaded panels," J. Acoust. Soc. Am. **92**, 1473-1488 (1992).

[13] B. J. Brévart and C. R. Fuller, "Radial impulsive excitation of infinite fluid-filled elastic cylindrical shells," J. Sound Vib. **177**, 411-422 (1994).

[14] M. Utschig, "A Traveling wave approach to study the dynamic response of a submerged cylindrical shell," MS Thesis, Northwestern University (1993).

[15] J. A. Mann, E. Williams, K. Washburn, and K. Grosh, "Time-domain analysis of the energy exchange between structural vibrations and acoustic radiation using near-field acoustical holography measurements," J. Acoust. Soc. Am. **90**, 1656-1664 (1991).

[16] A. V. Oppenheim and R. W. Schafer, Discrete-time signal processing (Prentice-Hall, Englewood Cliffs, NJ, 1989).

[17] S.-H. Choi, J. D. Achenbach, and T. Igusa, "The effect of periodically attached substructures on the excitation of submerged cylindrical shells," J. Sound Vib. **177**, 379-392 (1994).

[18] Y. P. Guo, "Radiation from cylindrical shells driven by on-surface forces," J. Acoust. Soc. Am. **95**, 2014-2021 (1994).

[19] M. C. Junger and D. Feit, *Sound, Structures and their Interactions*, 2nd edition (The MIT Press, Cambridge, MA, 1986).